Chapter 3

The Basic Theory of X-ray Fluorescence and Inductively Coupled Argon Plasma

3.1 The History of X-ray Fluorescence Spectroscopy

The accidental discovery of X-rays in 1895 by the German physicist, Wilhelm Conrad Roentgen; spurred the study of the X-ray fluorescence spectroscopy for identifying the characteristic of element. While he was studying cathode rays in a high-voltage, gaseous-discharge tube, Roentgen observed that even though the experimental tube was encased in a black cardboard box the barium-platinocyanide screen, which was lying adjacent to the experiment, emitted fluorescent light whenever the tube was in operation. However, the possible use of X-rays in analytical chemistry went unnoticed until 1913 (E. P. Bertin, 1978).

X-ray diffraction was first designed in 1912 with the classic experiment of Friedrich and Knipping, under the direction of Max von Laue (W. Friedrich, P.

Knipping and M. Von Laue, 1912) , in which the diffraction property of crystalline materials and the wave character of X-rays were confirmed for the first time.

Another scientist, Barkla, demonstrated that different "hardnesses" (a term used to denote penetrating power) of radiation were emitted, depending upon excitation and target characteristics (C. G. Barkla, 1911). It was in fact Barkla who proposed the line series nomenclature K, L, M, etc., still in use today.

In 1913, H.G.J. Moseley proved the relationship between atomic number Z and the reciprocal of the wavelength ($1/\lambda$) for each spectral series of emission lines for each element. He postulated it as "Moseley Law": (H. G. J. Moseley, 1912; 1913)

$$\mathbf{C / \lambda = a (Z - \sigma)^2}$$

Where **a** is a proportionality constant and σ is a constant dependent on the periodic series. Mosley also constructed the early X-ray spectrometer. He designed a hole centered around a cold cathode tube where the air within the tube provided the electrons and the analyte, which served as the tube target. However he encountered major problems of inefficiency in using electrons to create X-rays; nearly 99% of the energy was lost as heat (R. Jenkins, 1974).

In the same year, the Bragg brothers built their first X-ray analytical device. Their device was based around a pinhole and slit collimator. Like Moseley's instrument, the Braggs ran into difficulty in maintaining the efficiency of the X-ray device.

Progress in XRF spectroscopy continued in 1922 when Coster and Nishina put forward the idea of replacing electrons with x-ray photons to excite secondary x-

ray radiation resulting in the generation of x-ray spectra (D. Coster, and J. Nishina, 1925). This technique was also attempted by Glocker and Schrieber in 1928 (R. Glocker, and H. Schrieber, 1928).

Progress appeared to be at a standstill until 1948, when Friedman and Birks built the first XRF spectrometer. Their device was built around a diffractometer, with a Geiger Counter for a detection device and proved to be comparatively sensitive for much of the atomic number range (H. Friedman and L. S. Birks, 1948).

Within a decade, XRF became an important method of analysis for elements with atomic numbers greater than twenty-two. It might be noted that XRF spectrometers have progressed to the point where elements ranging from Beryllium to Uranium can now be analyzed.

The early commercial XRF devices was designed for the simple air path conditions, machines were soon developed utilizing helium or vacuum paths, permitting the detection of lighter elements. In the 1960's, the devices was improved by using lithium fluoride crystals for diffraction and chromium or rhodium target x-ray tubes to excite longer wavelengths. Then, the multi-channel spectrometers for the simultaneous measurement of many elements were developed. By the mid 60's computer controlled XRF devices were coming into use. In 1970, the lithium drifted silicon detector (Si(Li)) was made, providing very high resolution and X-ray photon separation without the use of an analyzing crystal. An XRF device was even included on the Appollo 15 and 16 missions.

3.2 The Principle of XRF

Characteristic X-rays consist of discrete wavelengths, which are the characteristic for the emitting element. On this basis, X-ray Fluorescence spectrometry is one of the most powerful methods to use for identifying the presence of an element by it's peak or series of peaks characteristic of that element. In general, each element has a unique x-ray signature that can be identified, and the number of x-rays emitted by the element can be qualified by their wavelength, and when impinged upon detectors, will quantify the amount of re-fluoresced X-rays. X-ray fluorescence is also a non-destructive method for identifying the material to such an extent that the raw materials may be analyzed qualitatively without any preparation.

In XRF spectroscopy, the process begins by exposing the element to a source of X-ray or gamma rays. As these high-energy photons strike the element, it may interact with the atoms of element by ejecting an orbital electron, such as K, L or M electron, leaving the atom ionized. Figure 3.1 shows the electron rearrangement in an atom which have been exposed to X-ray radiation generating a characteristic fluorescent X-ray.

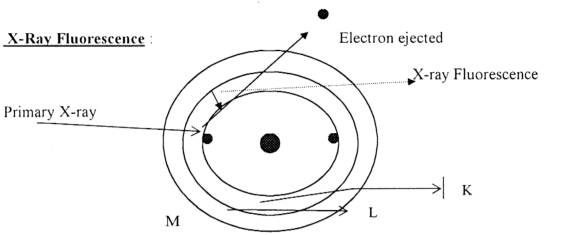

Figure 3.1: Electron rearrangement in an atom exposed to X-ray radiation generating a characteristic fluorescent X-ray.

In doing so, the atom now in an excited state; a vacancy is created in an orbit, an outer orbital of electron will fall down to fill the vacancy. Since outer orbital electrons are more energetic than inner shell electrons, the relocated electron has an excess of energy that is expended as an XRF in the form of electromagnetic radiation. This is also called characteristic radiation, i.e. characteristic of the atoms in the element and of the shells between which the transitions took place (N. A. Dyson, 1975). Figure 3.2 shows the very sharp spikes, which are called characteristic lines of an element.

Figure 3.3 shows x-ray emissions which are designated as K, L, or M, referring to the orbit that is ionized then filled, using the Bohr designations for the orbitals. For example, a K_α line is produced by a vacancy in the K shell filled by a L shell electron, whereas a K_β line is produced by a vacancy in the K shell filled by an M shell electron. K lines have the shortest wavelengths and, therefore, the highest energies. L lines have longer wavelengths and thus lower energies and M lines have very long wavelengths and thus even lower energies ($E \propto V_{freq.}$. $1/\lambda$).

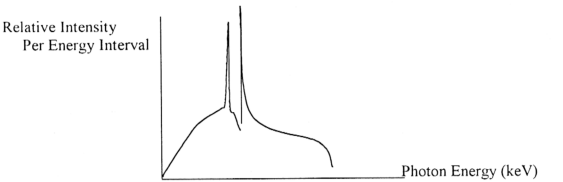

Figure 3.2: The very sharp spikes are called characteristic lines, and the X-radiation is termed characteristic radiation. These sharp lines are due to the electrons being knocked out of the K shell of an atom and then the electrons from the L shell cascading down into the vacancies in this K shell.

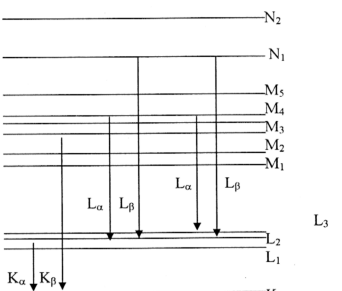

Figure 3.3: Production of K and L X-rays

However, for the above emission of characteristic X-ray fluorescent from an element, there have some weak lines accompany the strong characteristic X-ray photons were emitted. There are the radioactive Auger effect and Bremsstrahlung effect.

3.3 The Auger Process: Fluorescent Yield

This process is starting with removal of an inner shell atomic electron to form a vacancy by exposing to primary X-ray or gamma rays. Then the higher level of electron which is more energetic than inner shell electron will fall and relocated the vacancy. XRF simultaneously released. This XRF will occasionally absorb by the electron, and ejecting from the atom. This electron is called an Auger electron and appears with energy given by the difference between the original atomic excitation energy and the binding energy of the shell from which the electron was ejected. This Auger effect is actually reducing the yield of X-ray photons. The fluorescence yield (w) is the ratio of X-ray created in that shell; in other words, it meant the ratio of the numbers of Auger electrons and orbital electron vacancies produced in the same time and is equal to 1 - ω. Actually, ω varies with atomic number and line series. However, the Auger effect is more common in elements of low Z because their atomic electrons are more loosely bound and their characteristic X-rays more readily absorbed. For the case of lead, Pb, which has the atomic number 82, the impact of reducing the yield of X-ray photon is minimum in $_{82}$Pb analysis (E. P. Bertin, 1978; I. Adler, 1966). Figure 3.4 shows the Auger Effect on reducing the yield of X-ray photon.

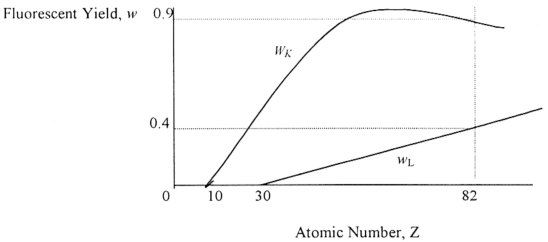

Figure 3.4: The Auger Effect on Reducing the Yield of X-ray Photon

3.4 Bremsstrahlung Effect:

The process of Bremsstrahlung (braking radiation) is the result of radioactive "collision" (interaction) between a high-speed electron and a nucleus. The electron while passing near a nucleus may be reflected from its path by the action of Coulomb Forces of attraction and lose energy as bremsstrahlung, a phenomenon which was predicted by Maxwell's general theory of electromagnetic radiation. As the electron, with its associated electromagnetic field, passes in the vicinity of a nucleus, it suffers a sudden deflection and acceleration. As a result, a part or all energy is dissociated from it and propagates in space as electromagnetic radiation (F. M. Khan, 1984).

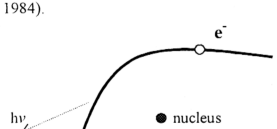

Although bremsstrahlung radiation can occur at any energy or wavelength it is often associated with X-ray region of the electromagnetic spectrum, a continuum spectrum. Since an electron may have more than one or more bremsstrahlung interactions in the material and an interaction may result in partial or compute loss of electron energy, the resulting bremsstrahlung may have any energy up to the initial energy of the electron. Also, the direction of emission of bremsstrahlung photons depends on the energy of the incident electrons. At electron energies below about 100 keV, X-rays are emitted more or less equally in all directions. Since these spectra are continua, they cannot be applied directly to the energy calibration of radiation detectors. Besides, for identify the shape of the energy spectrum emission from an X-ray fluorescence of an element, the bremsstrahlung effect can be altered by filtration or passage through appropriate absorber materials. Through the use of absorbers that preferentially remove the lower-energy photons, a peaked spectrum can be produced which, although far from mono-energetic, can be useful in identify the presence of an element and energy calibration of detectors.

The energy loss per atom by electrons depends upon the square of the atomic number (Z^2). Thus, the probability of Bremsstrahlung production varies with Z^2 of the target material. In other words, the electron energy converted into bremsstrahlung increases with increasing electron energy and is largest for absorbing materials of high atomic number, such as $_{82}Pb$.

In the following subsections, a detail discussion will be focused on the individual interaction of photons with matter. When penetrating matter, γ and X-rays

can interact with the atoms in various ways, namely photoelectric absorption, Compton scattering and pair production.

3.5 Photoelectric Effect

In the photoelectric absorption process, the photon interacts with a bound electron, and all of the photon energy is absorbed. In this case, the electron is removed from one of the internal shells of the atom. The fundamental equation of the photoelectric effect, which expresses the energy balance, is also valid (for photoelectric absorption on the K shell),

$$E=E_e^k + I_k \qquad [3.1]$$

where, E is the photon energy

E_e^k is the kinetic energy of the photoelectron knocked out of the K shell

I_k is the binding energy of the electron in the K shell.

The probability of the photoelectric effect occurring is larger when the photon energy is close to the binding energy (K-edge). Then, resonance sets in, and the cross section of the photoelectric effect is particularly large. Since the ejected electron leaves a hole in a shell of the atom, this atom will be de-excited with the emission of one or more characteristic X-ray or Auger electrons (E. P. Bertin, 1978)

As the photon energy increases relative to the value of I_k, the cross section decreases rapidly. A similar effect is produced by a decrease in the atomic number of the absorber, since here the binding energy of the internal electrons also decreases ($I_k \sim Z$). As a result of the fact that the K electrons, which are the closest to the nucleus, have a maximum binding energy, the photoelectric absorption on the K

shell for $E > I_k$ always predominates. Figure 3.5 shows the schematic graph for K- and L-edges. Photoelectric absorption in the subsequent shells, despite the large number of electrons they contain, is negligibly small. Theory also gives an equation for the photoelectric absorption cross section on the K shell when $E >> I_k$ as

$$T_{ak} = 10_{-23} \cdot Z^3 / E^3 \ (cm^2 / atom) \qquad [3.2]$$

E, is in MeV.

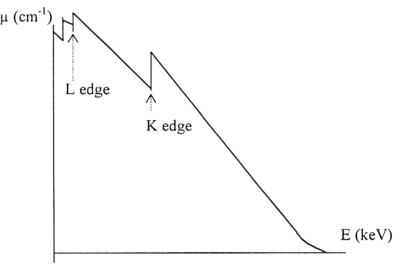

Figure 3.5: The Schematic Graph of K- and L-edges

3.6 Compton Scattering

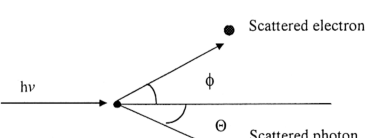

In the Compton scattering process, the photon energy, interacting with the weakly bound electrons, lose part of their energy and transfer it to the electrons in

the form of kinetic energy and momentum through inelastic scattering. So, established a connection between the energies of the primary X-ray E_{XR}, the scattered quantum $E_{XR'}$ and the electron E_e, and also their scattering angles relative to the direction of the primary quantum, namely Θ of the scattered quantum and ϕ of the electron as

$$E_{XR'} = E_{XR} / (1+ \alpha(1-\cos \Theta)) \qquad [3.3]$$

$$E_e = E_{XR} - E_{XR'} \qquad [3.4]$$

$$\text{Cot } \phi = (1+\alpha) \tan \Theta /2 \qquad [3.5]$$

Where $\alpha = E_{XR} / mc^2$, $mc^2 = 0.511$ MeV. For the energy distribution of the secondary electrons, there is a characteristic upper limit $E_e (max) = E_f - E_{f'} \mid_{\Theta=\pi} = E_f (2\alpha) / (1 + 2\alpha)$. *Coherent scattering is omitted because of the negligible energy transfer associated with it (Z.H., Cho, *et.al.*, 1993).

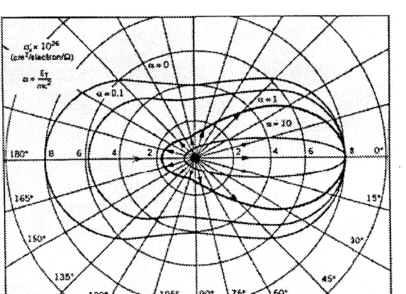

Figure 3.6: A Polar Diagram of the Differential cross section σ'_e

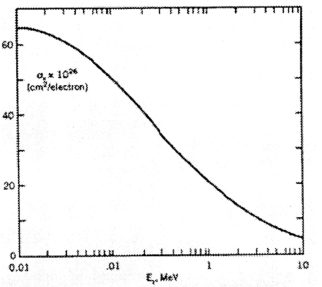

Figure 3.7: Energy σ'_e and σ_e are the differential and total cross section, respectively and Ω in the unit of solid angle

(Z.H., Cho, et.al., 1993)

As can be seen from the figure 3.6, the distribution of scattered photons becomes more and more forward peaked with increasing energy. The values presented are those of the differential cross section per electron per unit solid angle (cm^2 / electron / Ω).

The integral of the differential cross section over all possible angles gives the total cross section σ_e of the interaction, which is only a function of the energy. The dependence of the integral cross section σ_e, calculated per electron, on the energy is shown in figure 3.7. It has the form of a broad distribution, which decreases slowly with increasing energy. Thus, Compton interaction is probable for gamma quanta over a wide range of energies.

For almost all atomic electrons (with the exception of the K and L electrons in heavy atoms), the weak coupling condition is satisfied ($I_K \ll E_\gamma$). Therefore the

atomic cross-section for the Compton effect σ_a, calculated per atom, is equal to the product of σ_e and the number of atomic electrons; that is to say, $\sigma_a = \sigma_e Z$.

3.7 Pair Production

At very high photon energies, the photon can interact with the nucleus of an atom. The photon disappears and an electron and a positron emerge. These two particles lose their energy by ionization, until a positron is annihilated by an electron, with the generation of two identical photons. However, the cross section for pair production is not taking into account for the case of X-ray.

3.8 The Theoretical Model

To further confirm the experimental results, one set of theoretical model has been formed to calculate the total count of $K_{\alpha 1}$ (75 keV) line of Pb.

3.8.1 Simple Theory of the Model

A simple model had been built (as shown in figure 3.8) based on the established theory (E. P. Bertin, 1978) to calculate the count of the excitation of K x-rays of Pb. Below is the brief discussion of this theoretical model.

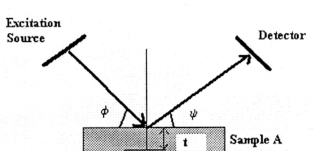

Figure 3.8: The Simple Schematic of the Excitation of XRF

1. Incident photon intensity: I_0 , λ_{pri}

2. Attenuation of the primary beam in reaching layer **t:**

$$\exp[- (\mu / \rho)_{A\,,\,\lambda pri} (\rho)(t) (\csc \phi)] \qquad [3.6]$$

(μ: mass-absorption coefficient)

1. Probability of excitation of analyte line K:

$$\frac{C_A (\mu / \rho)_{A\,,\,\lambda pri}}{(\mu / \rho)_{m\,,\,\lambda pri} [(r_A - 1) / r_A] (\omega_A) (g_k) (d\Omega / 4\pi) \exp [- (\mu / \rho)_{m\,,\,\lambda pri} (\rho)(t)(\csc \phi)]} \qquad [3.7]$$

where

C_A: weight fraction , $[(r_A - 1) / r_A]$: absorption edge jump ratio, ω_A: fluorescence yield of Pb

$$g_k = \frac{I_{k\alpha 1} + I_{k\alpha 2}}{\sum I_k}$$

g is the fractional value or relative intensity of the analyte A line in its series, or the probability of the orbital electron transition causing the analyte A line, or the fraction of the total K-series X-ray photons emitted by the analyte A that are Kα photons. $\sum I_k$ is the sum of the intensities of all the analyte A's K lines, including $K_{\alpha 1} + K_{\alpha 2}$.

2. Fraction of analyte-line photons emitted toward source collimator:

$$\frac{d\Omega}{4\pi} \qquad [3.8]$$

3. Attenuation of this analyte-line radiation in emerging from the specimen:

$$\exp [- (\mu / \rho)_{m\,,\,\lambda L} (\rho) (t) (\csc \psi)] \qquad [3.9]$$

Combination of all these expressions gives the analyte-line intensity ΔI_L emitted from layer t that actually enters the source collimator:

$$\Delta I_L = \frac{I_{0,\lambda pri} \{ \exp [- (\mu / \rho)_{A,\lambda pri} (\rho) (t) (\csc \phi)]\} (\mu / \rho)_{A,\lambda pri} (\rho) (t) (\csc \phi) C_A (\mu / \rho)_{A,\lambda pri}}{(\mu / \rho)_{m,\lambda pri} [(r_A - 1) / r_A] (\omega_A) g_k (d\Omega/4\pi) \exp [- (\mu / \rho)_{m,\lambda pri} (\rho) (t) \csc \psi]} \quad [3.10]$$

Or after simplify the equation above, becomes:

$$I_L = \{I_{0,\lambda pri} [(r_A - 1) / r_A] (\omega_A) (g_k) [d\Omega / 4\pi]\} \frac{C_A (\mu / \rho)_{A,\lambda pri} [\rho \csc\phi]}{(\mu / \rho)_{m,\lambda pri} [\rho \csc\phi] + (\mu / \rho)_{m,\lambda L} [\rho \csc \psi]} \quad [3.11]$$

If we define:

$$P_A = \omega_A g_k [(r_A - 1) / r_A] (d\Omega / 4\pi) \quad [3.12]$$

And

$$A = \frac{\text{Sin } \phi}{\text{Sin } \psi} \quad [3.13]$$

So,

$$I_K = P_A I_{0,\lambda pri} C_A \{ \frac{(\mu / \rho)_{A,\lambda pri}}{(\mu / \rho)_{m,\lambda pri} + (\mu / \rho)_{m,\lambda K}} \} \quad [3.14]$$

The equation above regarded as the fundamental excitation equations (intensity formula) for secondary x-ray excitation with monochromatic primary X-radiation. These equations are valid only for smooth homogeneous specimens, for collinear primary beams and in the absence of multiple scatter and enhancement effects.

P_A regarded as an excitation factor, A is a geometric factor, and the fractional term as an efficiency factor. P_A is constant for a given analyte A, matrix, and

spectrometer, including a specified set of components. A influences the relative importance of absorption of the primary and secondary (analyte-line) X-rays. At low take-off angles ψ, A becomes large, and secondary absorption predominates. This relationship is useful in excitation by continuous spectra because secondary absorption effects apply to the monochromatic analyte line λ_K, so calculations are much simpler than when absorption of the primary continuum predominates.

If the analyte line is excited by a polychromatic continuos X-ray beam rather than a monochromatic beam, it is necessary to consider all incident wavelengths between the short wavelength limit λ_{min} and the absorption edge λ_{ab} associated with the analyte line. One must consider the spectral distribution of this region and the mass-absorption coefficient of the specimen for each wavelength in this region.

The spectral distribution **J** (λ_{pri}) is the plot of the intensity of each wavelength in the effective region between λ_{min} and λ_{ab} . This distribution may be measured, calculated, replaced with a monochromatic effective wavelength λ_{eff} or corrected for by means of influence coefficients. When excitation is predominantly by continuum, the effective wavelength is given by

$$\lambda_{eff} \approx (2/3)\,\lambda_{ab} \qquad [3.15]$$

When excitation is predominantly by target-line X-rays $\lambda_{K\text{-target}}$,

$$\lambda_{eff} \approx \lambda_{K\text{-target}} \qquad [3.16]$$

The value of λ_{eff} is not critical, and difference of ±25% only has little effect on the calculations.

Mass-absorption coefficients must be considered for all elements in the specimen matrix for all effective primary wavelengths and for the analyte line. Expressions of the following form are obtained:

$$(\mu / \rho)_{M, \lambda pri} = \sum C_i (\mu / \rho)_{i, \lambda pri} \qquad [3.17]$$

$$(\mu / \rho)_{M, \lambda K} = \sum C_i (\mu / \rho)_{i, \lambda K} \qquad [3.18]$$

Where $(\mu / \rho)_{M, \lambda pri}$ and $(\mu / \rho)_{M, \lambda K}$ are mass-absorption coefficients of the specimen for a specific primary wavelength λ_{pri} and the analyte line λ_K; $(\mu / \rho)_{i, \lambda pri}$ and $(\mu / \rho)_{i, \lambda K}$ are mass-absorption coefficients of a specific element I for λ_{pri} and the λ_K; and C_i is concentration of element i (weight fraction). In these equations, i include A, the analyte. Therefore,

$$I_K = P_A C_A \int J(\lambda_{pri}) (\mu / \rho)_{A, \lambda pri} \left\{ \frac{1}{\sum C_i [(\mu / \rho)_{i, \lambda pri} + (\mu / \rho)_{i, \lambda K}]} \right\} d\lambda \qquad [3.19]$$

which integrate from λ_{min} to λ_{ab}. The application of this model is shown in chapter 5.

3.9 The Basic Principle of ICP-AES

Since the Inductively Coupled Plasma (ICP) development in the early sixties, it has been considered as an excellent laboratory tool for such application as spheroidization, chemical synthesis, nuclear rocket simulation, and extractive metallurgy. One of its wide applications has been as an emission source in spectra-chemical analysis in which it is being increasingly used on a commercial basis. Two

comprehensive reviews on the subject have been published by Eckert (1974) and Barnes (1978).

ICP is designed to generate plasma, which is a gas in which atoms are present in an ionized state. The temperature is within 7000-8000K-excitation source that efficiently desolvated, vaporizes, excites, and ionizes atoms. Molecular interference is greatly reduced with this excitation source but are not limited completely (J. M. Mermet, and C. Trassy, 1980). The basic set-up of an ICP consists of three concentric tubes, most often made of silica. These tubes, termed outer loop, intermediate loop and inner loop, collectively make up the torch of the ICP. The torch is situated within a water-cooled coil of a radio frequency (r.f.) generator. As flowing gases are introduced into the torch, the r.f. field is activated (typically 1-5 kW @ 27 MHz or 41 MHz) and the gas in the coil region is made electrically conductive. This sequence of events forms the plasma. The formation of the plasma is dependent upon an adequate magnetic field strength and the pattern of the gas streams follows a particular rotationally symmetrically pattern. The plasma is maintained by inductive heating of the flowing gases. The induction of a magnetic field generates a high frequency annular electric current within the conductor. The conductor, in turn, is heated as the result of its ohmic resistance (Boumans, 1987). Figures 3.9, 3.10 and 3.11 show a typical schematic of plasma torch, the plasma flame and the schematic of ICP flames respectively. Figure 3.12 shows a schematic cross-section of an ICP.

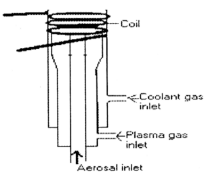

Figure 3.9: A typical Plasma Torch

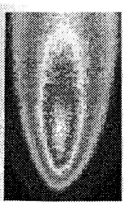

Figure 3.10: The Plasma Flame

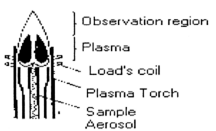

Figure 3.11: Schematic of ICP Flames

In order to prevent possible short-circuiting as well as meltdown, the plasma must be insulated from the rest of the instrument. Insulation is achieved by the concurrent flow of gasses through the system. Three-gas flow through the system—there are outer gas, intermediate gas, and inner or carrier gas. The outer gas is typically Argon or Nitrogen. The outer has been demonstrated to serve several purposes including maintaining the plasma, stabilizing the position of the plasma, and thermally isolating the plasma from the outer tube. Argon is commonly used for both the intermediate gas and inner or carrier gas. The purpose of the carrier gas is to convey the sample to the plasma.

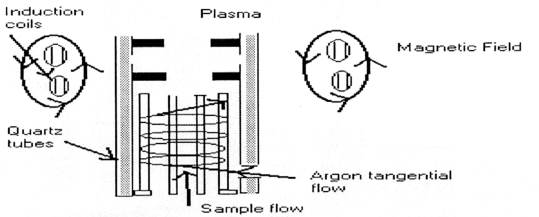

Figure 3.12: A Schematic Cross-section of an ICP

3.10 ICP Main Components

The main components of an ICP are:

- Sample introduction system (nebulizer)
- ICP torch
- High frequency generator
- Transfer optics and spectrometer
- Computer interface

An ICP requires that the elements, which are to be analyzed, be in solution. An aqueous solution is preferred over an organic solution, as organic solutions require special manipulation prior to injection into the ICP. Solid samples are also discouraged, as clogging of the instrumentation can occur. The nebulizer transforms the aqueous solution into an aerosol. The light emitted by the atoms of an element in the ICP must be converted to an electrical signal that can be measured quantitatively. This is accomplished by resolving the light into its component radiation (nearly always by means of a diffraction grating) and then measuring the

light intensity with a photomultiplier tube at the specific wavelength for each element line. The light emitted by the atoms or ions in the ICP is converted to electrical signals by the photomultiplier in the spectrometer. The intensity of the electron signal is compared to previous measured intensities of known concentration of the element and a concentration is computed. Each element will have many specific wavelengths in the spectrum that could be used for analysis. Thus, the selection of the best line for the analytical application in hand requires considerable experience of ICP wavelengths.

3.11 Advantages and Disadvantages

Advantages of using an ICP include its ability to identify and quantify all elements with the exception of Argon; since many wavelengths of varied sensitivity are available for determination of any one element. The ICP is suitable for all concentration from ultratrace levels to major components; detection limits are generally low for most elements with a typical range of 1-100g/L. Probably the largest advantage of employing an ICP when performing quantitative analysis is the fact that multielemental analysis can be accomplished, and quite rapidly. A complete multi-element analysis can be undertaken in a period as short as 30 seconds, consuming only 0.5 ml of sample solution. Although in theory, all elements except Argon can be determined using and ICP, certain unstable elements require special facilities for handling the radioactive fume for the plasma. Also, an ICP has difficulty handling halogens—special optics for the transmission of the very short wavelengths become necessary.

3.12 Combining ICP with Atomic Emission Spectroscopy

Often, ICP is used in conjunction with other analytical instruments, such as the Atomic Emission Spectroscopy (AES) and Mass Spectroscopy (MS).

ICP-AES has been widely used since the 1970's for the simultaneous multi-element analysis of environment and biological samples after dissolution. The simple schematic of ICP system is shown in figure 3.13. The excellent sensitivity and wide working range for many elements-together with the low level of interference, make ICP-AES a nearly ideal method so long as sample throughput is high enough to justify the initial capital outlay.

ICP-AES has been approved for the determination of metals by the EPA under Method 6010. Method 6010 describes the simultaneous, or sequential, multielemental determination of elements by ICP-AES. This method is approved for a large number of metals and wastes. All matrices, including ground water, aqueous samples, EP extracts, industrial wastes, soils, sludge, sediments, and other solid wastes, require digestion prior to analysis (EPA Method 6010, 1986)

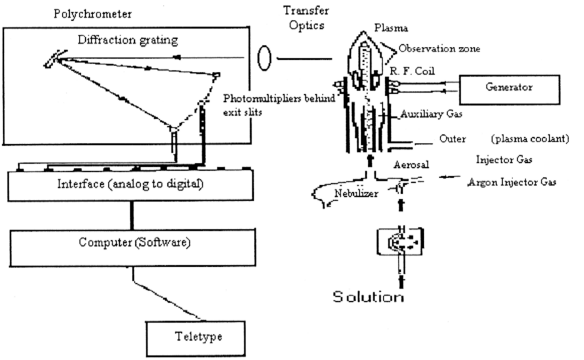

Figure 3.13: A Schematic of ICP System

References:

Bakla, *Phil. Mag.*, vol.21, p. 648 (1911).

Boumans, P.W.J.M., 1987, *Inductively Coupled Plasma-Emission Spectroscopy,* Part I, John Wiley & Sons, New York, pg. 584.

D. Coster, and J. Nishina, 1925, *Chem. News.*, 130, 149.

E. P. Bertin, 1978, *Introduction to X-ray Spectrometric Analysis;* Plenum Press: New York and London, pg. 1-3; 50-51; 78-80; 129-132.

EPA Method 6010. Revision date: September 1986.

F. M. Khan, 1984, *The Physics of Radiation Therapy,* Williams & Wilkins, p.34-35.

H. Friedman, and L. S. Birks, 1948, Rev. Sci. Instr. 19, 323.

H. G. J. Moseley, *Phil.Mag.26,* 1024 (1912); 27, 703 (1913).

H. U. Eckert, 1974, *High Temp. Sc.*, 6, 99.

I. Adler, 1966, *X-Ray Emission Spectrography in Geology,* Elsevier Publishing Company, pg. 26-28.

J. M. Mermet, and C. Trassy, 1980, *Spectral Interferences with an ICP in Atomic Emission Spectroscopy.*, International Winter Conference San Juan, Puerto Rico, p.61-67.

N. A. Dyson, 1975, *Characteristic X-rays—A still Developing Subject*, Phys.Med.Biol., vol.20, No.1, 1-29.

R. Glocker, and H. Schrieber, 1928, *Ann. Physik 85,* 1085.

R. Jenkins, 1974, "*An Introduction to X-ray Spectrometry*"; Heyden and Sons Ltd, p.4.

R. M. Barnes, 1978, *CRC Crit. Rev.*, Anal. Chem., 7, 203.

W. Friedrich, P.Knipping and M.Von Laue, *Proc.Bavarian Acad.Sci,* 1912, 303; Reprinted in Naturewissenschaften, 1952, 39, 367.

Z.H. Cho, J.P. Jones and M. Singh, 1993, *Foundations of Medical Imaging,* John Wiley & Sons, pg. 112-114.